

4-D Micro-CT of the Mouse Heart

Cristian T. Badea, Boma Fubara, Laurence W. Hedlund, and G. Allan Johnson

Duke University Medical Center

Abstract

Purpose: Demonstrate noninvasive imaging methods for in vivo characterization of cardiac structure and function in mice using a micro-CT system that provides high photon fluence rate and integrated motion control. **Materials and Methods:** Simultaneous cardiac- and respiratory-gated micro-CT was performed in C57BL/6 mice during constant intravenous infusion of a conventional iodinated contrast agent (Isovue-370), and after a single intravenous injection of a blood pool contrast agent (Fenestra VC). Multiple phases of the cardiac cycle were reconstructed with contrast to noise and spatial resolution sufficient for quantitative assessment of cardiac function. **Results:** Contrast enhancement with Isovue-370 increased over time with a maximum of ~500 HU (aorta) and 900 HU (kidney cortex). Fenestra VC provided more constant enhancement over 3 hr, with maximum enhancement of ~620 HU (aorta) and ~90 HU (kidney cortex). The maximum enhancement difference between blood and myocardium in the heart was ~250 HU for Isovue-370 and ~500 HU for Fenestra VC. In mice with Fenestra VC, volumetric measurements of the left ventricle were performed and cardiac function was estimated by ejection fraction, stroke volume, and cardiac output. **Conclusion:** Image quality with Fenestra VC was sufficient for morphological and functional studies required for a standardized method of cardiac phenotyping of the mouse. *Mol Imaging* (2005) 4, 1–7.

Keywords: Micro-CT, resolution, mouse, phenotyping, cardiac imaging.

Introduction

Research on small-animal models of human cardiovascular disease is critical to our understanding of the origin, progression, and treatment of the disease—the leading cause of death in the United States [1] and a major cause of death worldwide [2]. The mouse is a commonly studied animal for such research because of the large, established information on its genetic make-up, its rapid rate of reproduction, and relatively low husbandry costs. However, its small size presents severe challenges for morphological and functional analysis. The cardiovascular system, in particular, has been difficult to analyze because of the small size of the heart (~7 mm long axis in the adult), and rapid heart rate (approximately 500 bpm) [3]. MR microscopy has been used to assess cardiac morphology and function in rodents [4–6] using specialized hardware, optimized

pulse sequences, and specific monitoring and gating systems adapted to the requirements of small and rapidly beating mouse and rat hearts [4,5,7]. The disadvantages of MR microscopy are related to the poor signal-to-noise ratio (SNR), long acquisition time, and high cost.

In vivo heart imaging is also possible and was performed in rats using micro-PET [8] and pinhole-gated SPECT [9], but the resolution of about 1 mm is not acceptable when imaging mice. On the other hand, echocardiography is the method of choice for cardiac function estimation [10]. However, echocardiography still uses a model-based estimation of the left ventricle volumes used in cardiac measure computations that rely on geometric assumptions that work well only in normal hearts [11]. An alternative imaging method that could be of interest is CT, but to our knowledge micro-CT has not yet been used to image the mouse heart in vivo. Recent reports have suggested that such a feat would be “impossible with the state of the art technology” [12]. Thus, the purpose of this work was to design a micro-CT-based imaging technique appropriate for in vivo characterization of cardiac structure and function in mouse models of cardiovascular disease. We have developed a prototype micro-CT system with a design that addresses two of the most significant barriers to micro-CT in small animals, namely, the reduced SNR imposed by the smaller voxels and motion [13,14]. The most direct approach to increasing the SNR is to increase the total fluence rate. It is not possible to significantly increase the fluence rate in most of the laboratory and commercial micro-CT systems currently in use [15–17] because these systems use small fixed focal spot tubes. One can integrate over extended periods with these devices, but then biological motion poses the resolution limit. Our system allows the use of high X-ray photon fluence with integrated physiologic monitoring and control of breathing and cardiac motion.

Corresponding author: G. Allan Johnson, PhD, Center for In Vivo Microscopy, Duke University Medical Center, Box 3302, Durham, NC 27710, USA; e-mail: gaj@orion.duhs.duke.edu.

© 2005 BC Decker Inc

We present here cardiac micro-CT methods tailored for the mouse sufficient to achieve isotropic resolution (100 μm) for in vivo images of cardiac structure and function with a temporal resolution of 10 msec. We explored two approaches to increase the contrast between myocardium and blood: (a) a conventional iodinated contrast agent Isovue-370 mg/mL iodine (trademark of Bracco Diagnostics, Princeton, NJ) given as a constant infusion during sampling, and (b) a new generation of a blood pool contrast agent containing iodine in a concentration of 50 mg/mL Fenestra VC (Alerion Biomedical, San Diego, CA). Isotropic volume images of the mouse heart are shown at multiple points of the cardiac cycle. Based on volumetric measurements of the left ventricle in end-systole and end-diastole, the cardiac function parameters such as ejection fraction (EF), stroke volume (SV), and cardiac output (CO) were computed.

Materials and Methods

We exploited methods developed previously for magnetic resonance microscopy, where acquisition of the individual projections is synchronized to both the cardiac and the ventilation cycles [18]. The gating sequence corresponding to the R peak in the ECG cycle is presented graphically in Figure 1. An acquisition window of 100 msec was defined at a specific phase of the ventilation cycle (i.e., at end-expiration). The end-expiration phase of ventilation is longer than the period of inspiration and held breath to ensure more complete exhalation. Any QRS occurring within the window placed at end-expiration triggers an X-ray exposure. This ensured that the images were always acquired at the same

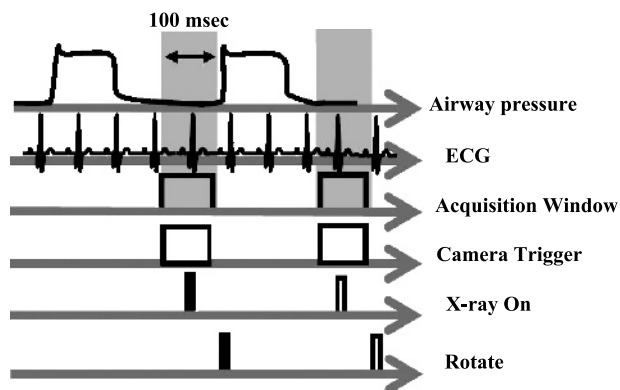


Figure 1. The gating sequence used to sample at end-expiration and fixed points during the cardiac cycle. Images corresponding to other points on the ECG cycle were acquired by sampling with a constant delay after detecting the R peak. A relatively constant heart rate ($\pm 8\%$) was maintained throughout each study.

phase of the cardiac cycle and within the same ventilation window at the same phase of breathing. Images at other points of the cardiac cycle were acquired by detecting the R peak and adding a constant delay. A relatively constant heart rate is assumed and was achieved by careful maintenance of the level of anesthesia and control of body temperature. For end-expiration, the beginning of the window was set to 420 msec after the beginning of the ventilation cycle. After a projection was acquired, the animal was rotated to the next scanning angle and the procedure was repeated. All studies were performed at 90 breaths/min (total breathing cycle = 666 msec).

Image Acquisition and Reconstruction

The micro-CT system, described in detail elsewhere [13,14], involves rotation of the vertically positioned animal and employs a stationary tube and an X-ray detector, which permits the use of a high flux rotating anode X-ray source (Philips SRO 09 50) with a dual 0.3/1.0 mm focal spot. The flux from the system is sufficient to support exposures as short as 10 msec to limit the motion blur from the heart. For example, the 1.0-mm focal spot can support 50 kW, more than 6000 \times that of commercial microfocus X-ray tubes. By using the stationary tube/detector with the rotating specimen, the geometric blur can be minimized giving a net usable flux increase at the detector of nearly 250 \times over commercial systems [14]. We employed a high-resolution detector (Microphotonics X-ray Image Star camera, Photonics Science, East Sussex, UK) with 50 \times 50 μm pixels covering an image matrix of 2048 \times 2048 over an active area input of 106 \times 106 mm. We used a hardware feature that binned pixels to a 2 \times 2 array that reduced the effective detector pitch to 100 μm .

X-ray parameters for volume imaging were typically 80 kVp, 150 mA, and 10 msec. Projections were acquired over a circular orbit of 189 $^\circ$ (i.e., 180 $^\circ$ + fan angle) with a step angle of 0.75 $^\circ$. A total of 252 projections were used. The scanning time for a complete projections set was 8–10 min depending on the synchronization between the ECG and ventilation, that is, sometimes, the QRS complex does not “occur” every bit in the window placed at end-expiration and the sampling time is increased. A recent investigation suggests that with the proposed gating procedure, the position of the heart and the diaphragm can be reliably reproduced through the course of a physiologically controlled study to ~ 100 μm [19]. Scanning was conducted with the animal placed at a source-to-object distance (SOD = 480 mm), an object-to-detector distance (ODD = 40 mm), and a source-to-detector distance (SDD = 520 mm), resulting in a

geometric blur of the focal spot that matched the Nyquist sample at the detector [14]. This resulted in measured exposure for each image set of 15.2 R. Thus, the absorbed dose in scanning 6 points in ECG cycle is 0.92 Gy. These projection images were used to reconstruct tomograms with a Feldkamp algorithm using Parker weighting [20]. For this purpose, we used the Cobra EXXIM software package (EXXIM Computing, Livermore, CA). Data were reconstructed as isotropic $1024 \times 1024 \times 1024$ arrays with effective digital sampling in the image plane of 90 μm , as the magnification factor for the geometry was 1.1.

To quantify the equivalent difference in concentration of iodine in the blood and myocardium provided by each contrast agent, we scanned a phantom containing tubes with various concentration of iodine (Isovue-370 mg/mL) diluted in water.

Animal Preparation

All animal studies were conducted under a protocol approved by the Duke University Institutional Animal Care and Use Committee. Studies were performed on C57BL/6 mice ($n = 10$) (Charles River Laboratories, Raleigh, NC) weighing between 25–30 g. Animals were anesthetized with 50 mg/kg ip of sodium pentobarbital and 2 mg/kg butorphanol. A catheter was placed in a lateral tail vein for contrast agent infusion, and following endotracheal intubation, anesthesia was maintained with 1–2% isoflurane. The influence of the injectable drugs was intended to be short acting and disappear after the animal setup, which takes ~ 50 min. The animals did not react in any negative way to the combination of injectables and the isoflurane. Anesthetic gas was delivered by a special purpose ventilator [21,22]. Using this device, the animals were mechanically ventilated at a rate of 90 breaths/min with a tidal volume of 0.4 mL. A solid-state pressure transducer on the breathing valve measured airway pressure and electrodes (Blue Sensor, Medicotest, UK) taped to the animal footpads

acquired ECG signal. Both signals were processed with Coulbourn modules (Coulbourn Instruments, Allentown, PA) and displayed on a computer monitor using a custom-written LabVIEW application (National Instruments, Austin, TX). Body temperature was recorded using a rectal thermistor and maintained at 36.5°C by an infrared lamp and feedback controller system (DigiSense, Cole Parmer, Chicago, IL). The animals were placed in an acrylic cradle in a vertical position with flexible umbilicus carrying breathing gas and physiologic signals suspended from above to allow free rotation.

Five mice ($n = 5$) were imaged during constant infusion of 1 mL Isovue-370 contrast agent delivered for 1 hr using an infusion pump (PEGASUS GMBH model Vario). One CT dataset was acquired for each animal before infusion, and four datasets were acquired during infusion at fixed points of the cardiac cycle (0, 25, 40, and 80 msec after the R peak).

The blood pool contrast agent Fenestra VC consists of iodinated triglycerides formulated in a stable, submicron oil-in-water lipid emulsion [23,24] containing iodine in a concentration of 50 mg/mL. We injected a single bolus of 0.5 mL/25 g mouse and scanned five mice ($n = 5$). Because the half-life of the blood pool agent was much longer than that of the Isovue-370, it was possible to sample the cardiac cycle more fully. One CT dataset was acquired before injection and six postinjection datasets were acquired at fixed points in the cardiac cycle (adding delays of multiples of 15 msec from the R).

After reconstruction, we used the public domain software ImageJ (National Institute of Mental Health, Bethesda, MD) to manually segment and assess the volume of the left ventricle in all images at systole and diastole.

Results

Figure 2 presents a comparison of similar axial slices through the heart for mice with (A) no contrast, (B)



Figure 2. A comparison of similar axial images acquired in diastole using (A) no contrast, (B) Isovue-370 after 1 hr of 1 mL/hr infusion, and (C) Fenestra VC, 1 hr postinjection. The images are windowed the same for objective comparison of contrast.

Isovue-370, and (C) Fenestra VC. All images were windowed in the same way for an objective comparison of enhancement. The Isovue-370 and Fenestra images were acquired 1 hr postcontrast administration (i.e., at the end of the infusion period for Isovue-370), and 1 hr postinjection for Fenestra.

The enhancements relative to noncontrast images were assessed on images of several important organs and presented in Figures 3 and 4 as a function of time starting from contrast agent administration. Mean values and standard deviation for $n = 5$ in each case are shown. Contrast enhancement increased with time for Isovue-370 (Figure 3), with a maximum mean enhancement of ~ 500 HU in the aorta and 900 HU in the kidney cortex. Fenestra VC provided a relatively constant enhancement over 3 hr with a maximum in the aorta of ~ 620 HU and in kidney cortices of only 90 HU. The relative differences in CT numbers between the myocardium and the blood in the ventricles corresponding to constant infusion of Isovue-370 increased as more contrast agent was accumulated in the blood. The maximum difference between blood and the myocardium in the heart was ~ 250 HU for Isovue-370 and was reached at the end of 1 hr of infusion. The Fenestra VC provided a relatively constant enhancement between blood in the ventricles and the myocardium of ~ 500 HU during 3 hr of sampling. A comparison of the cortex enhancement of the kidneys in Figures 3 and 4 shows that there is very little kidney enhancement and thus renal clearance with Fenestra VC compared with the Isovue-370. On the other hand, with Fenestra VC, the spleen shows an increasing enhancement over time that reaches a maximum of ~ 270 HU after 3 hr.

Figures 5 and 6 present results with the Fenestra VC contrast agent. Figure 5 shows axial slices through the mouse heart during six phases of the cardiac cycle

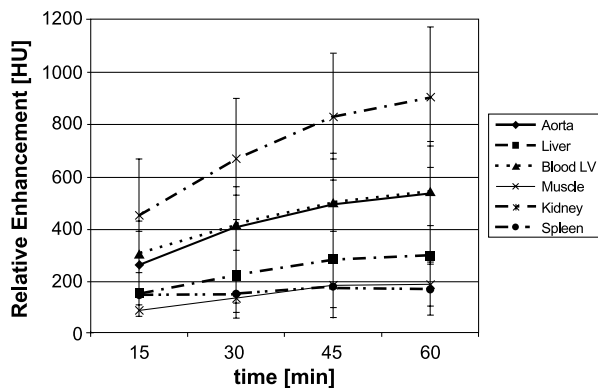


Figure 3. Enhancement relative to the noncontrast images for Isovue-370. The graph shows the mean and standard deviation for five mice. The datasets were acquired during 1 hr infusion of 1 mL Isovue-370.

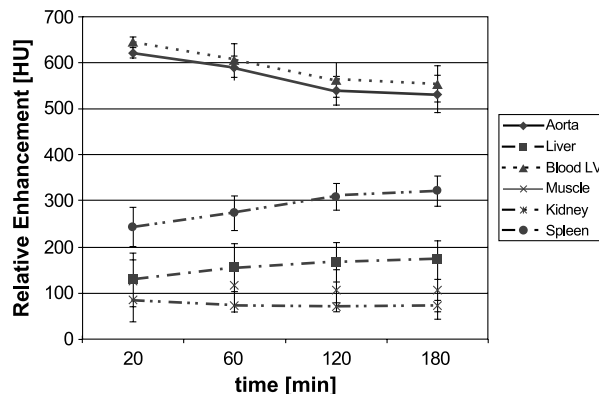


Figure 4. Enhancement relative to the noncontrast images for Fenestra VC. The graph shows the mean and standard deviation for five mice. **113**

at (A) 0, (b) 15 msec, (C) 30 msec, (D) 45 msec, (E) 60 msec, and (F) 90 msec delay after the R peak. Axial, coronal, and sagittal slices extracted from a 1024^3 volume acquired in diastole (90 msec delay after R peak) are displayed in Figure 6. The images are registered, that is, horizontal lines in (A) indicate the level of the coronal slice shown by (B), and the vertical lines in (A) indicate the sagittal plane shown by (C). Many anatomical details are visible.

Based on the calibration phantom, we determined that the constant infusion of Isovue-370 produced a contrast difference between the myocardium and the blood corresponding to 3.3–4.0 mg/mL difference in iodine concentration. In case of Fenestra VC, we obtained an equivalent difference in concentration of iodine ranging from 7.4 to 9.2 mg/mL during the experiment. Because of the superior contrast enhancement provided by Fenestra VC, quantitative estimation of cardiac function was made based on images with this contrast agent. EF, SV, and CO were computed based on the left ventricle volume measurement at systole and diastole. The results characterizing cardiac function obtained by analyzing five image sets with Fenestra VC are shown in Table 1.

Discussion and Conclusions

In the absence of physiologic control, breathing and cardiac motion produce streak artifacts and blurring that severely degrade the image quality of any CT studies in the thorax. In this study, these artifacts have been avoided by cardiac gating with ventilatory synchronization. Furthermore, in the case of constant infusion of Isovue-370, the amount of contrast agent in the blood increased over time, but as shown by our images (see Figure 2B), the image quality was not affected by artifacts suggesting that the concentration of contrast was

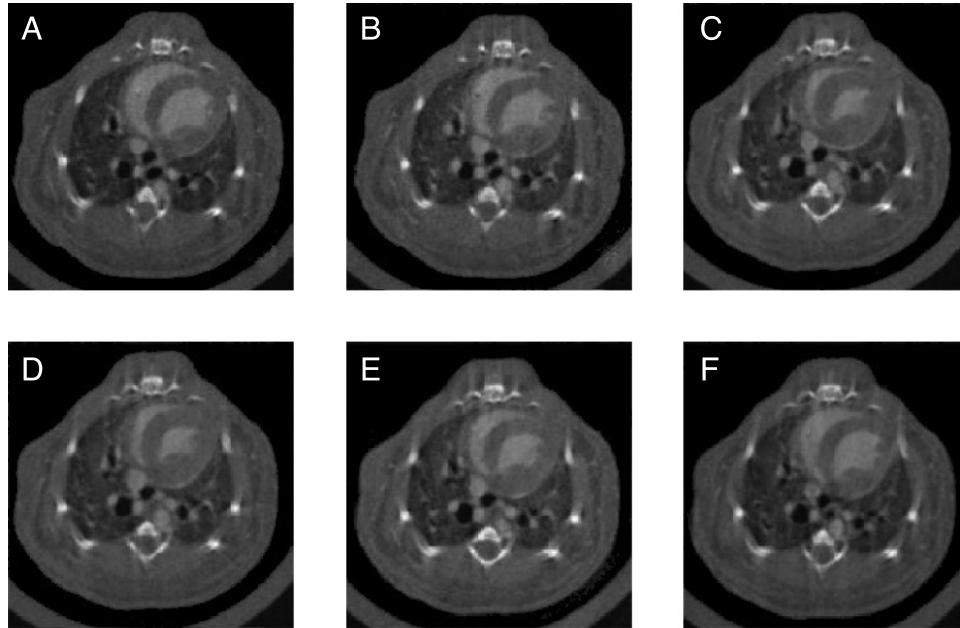


Figure 5. Axial slices through the mouse heart during six phases of the cardiac cycle at (A) 0, (B) 15, (C) 30, (D) 45, (E) 60, and (F) 90 msec after the R peak. All images were acquired using the Fenestra VC blood pool contrast agent.

relatively constant over an 8–10 min scan of any specific projection set. According to the Rose criterion [25], the detectable signal difference must be at least three to five times greater than the standard deviation in the image (i.e., noise which is ~ 50 HU with our system). In the case of Isovue-370, we see that during 1 hr infusion the signal difference between blood in the left ventricle and the myocardium is 2 to 4.6 times greater than noise reaching detectability in the second part of the experiment. In the case of Fenestra VC, the signal difference between blood and the myocardium is even greater (6.5 to 9.3), allowing successful imaging during the whole experiment.

As shown by Figures 3 and 4, the standard deviation of the enhancement in all experiments is much larger for Isovue-370 than for Fenestra VC, partly due to the fact that the infusion rate was not scaled with the animal

weight. Much more repeatable values for relative enhancements were obtained when using Fenestra VC. The relatively low enhancement between blood and the myocardium and the large volume required and its potential toxicity are factors that make Isovue-370 less desirable.

From the measurements of ventricular 3-D volumes at different points of the cardiac cycle, one can assess the cardiac function. Because voxels are isotropic, ventricular volumes can be measured at different phases of the cardiac cycle to support assessment of EF/CO and wall dynamics. Gated CT can be used for dynamic applications involving the heart, such as regional myocardial contraction determinations, including left ventricular wall thickening during the cardiac cycle. Our current efforts are dedicated to the analysis of the wall dynamics. Changes in wall thickening may be the most sensitive



Figure 6. (A) Axial, (B) coronal, and (C) sagittal slices through the mouse heart. The images are registered, namely, horizontal lines in (A) indicate the level of the coronal slice shown by (B), and the vertical lines in (A) indicate the sagittal plane shown by (C). Images were acquired in diastole using the Fenestra VC blood pool contrast agent. Many anatomical details are visible. Note, left ventricle (LV), right ventricle (RV), ascending aorta (AO), azygous (A), left main bronchus (MB) with peribronchial vessels, small bronchial pulmonary vessels, interventricular septum (S).

Table 1. Cardiac Function Estimation in Mice ($n = 5$) Using the Micro-CT

Cardiac Parameter	
LV diastolic vol [μ L]	49 \pm 10.7
LV systolic vol [μ L]	24 \pm 3.8
Heart rate [beats/min]	507 \pm 20.9
Ejection fraction [%]	50.9 \pm 2.8
Stroke volume [μ L]	25 \pm 6.3
Cardiac output [mL/min]	12.62 \pm 2

index of myocardial ischemia [26]. Our cardiac measures (e.g., EF \sim 50%), is very close to those reported with echocardiographic assessment for anesthetized mice with pentobarbital where EF = 52.6% \pm 2% [10]. On the other hand, a comparison with the MR-based published data [4] shows a 10% difference in EF. Our lower EF value could be related to the vertical position of the animal during scanning, which will cause a reduced venous return and a decrease in cardiac function.

We have compared a conventional iodinated contrast agent (Isovue-370) with Fenestra VC, a new class of blood pool contrast agent for CT with prolonged vascular residence time [23,27]. The blood pool contrast agent yielded excellent visualization of the cardiac structure, whereas the conventional iodinated contrast agents were less successful because of the rapid renal clearance and extravascular diffusion. The resulting images provide excellent delineation between the myocardium and blood, which allows relatively easy segmentation. The radiation dose associated with most micro-CT methods is significant. In the application reported here, the dose is a few times under the mouse lethal dose that ranges from 5.0 to 7.6 Gy [28]. We are exploring a number of interesting possibilities for dose reduction that we draw from MR literature where one exploits the redundancy of the spatio-temporal data [29–31]. To date, the majority of the imaging studies of cardiac physiology in murine models have used magnetic resonance imaging (MRI). The soft tissue contrast in MRI is a powerful attribute. But the combination of a high flux X-ray tube, careful physiologic gating, and the use of blood pool contrast agents has resulted in image sets with voxels of $1 \times 10^{-3} \text{ mm}^3$, roughly 10–50 times higher spatial resolution than has been seen with MRI [5,6].

Recently, General Electric has introduced a volumetric micro-CT scanner that offers the advantage of a rapid scanning 4s/8s and utilizes a dual digital flat-panel detectors and is coupled to a high-performance CT X-ray tube. Based on data provided by Ref. [32], this system is able to scan with similar parameters as ours but with a reduced resolution along the z -axis of

200 μ m. In conclusion, we consider that micro-CT will clearly play a role in the increasing need for imaging methods for structural and functional phenotyping in the mouse.

Acknowledgments

We thank Dr. Douglas Bakan of Alerion Biomedical for making the Fenestra VC contrast agent available and for numerous helpful suggestions. We also thank Sally Zimney for editorial assistance. All work was performed at the Duke Center for In Vivo Microscopy, an NIH/NCRR National Resource (P41 RR05959). Additional support was provided by NCI (R24 CA-92656) and the Department of Defense (DoD-556450).

References

- Minino A, Smith B (2001). Deaths: Preliminary data for 2000. In: *National vital statistics reports*. National Center for Health Statistics, Hyattsville, MD.
- Organization WH (2001). *World health report*. World Health Organization, Geneva.
- James J, Hewett T, Robbins J (1998). Cardiac physiology in transgenic mice. *Circ Res*. **82**:407–415.
- Wiesmann F, Ruff J, Hiller KH, Rommel E, Haase A, Neubauer S (2000). Developmental changes of cardiac function and mass assessed with MRI in neonatal, juvenile, and adult mice. *Am J Physiol Heart Circ Physiol*. **278**:H652–H657.
- Wiesmann F, Szimtenings M, Frydrychowicz A, Illinger R, Hunecke A, Rommel E, Neubauer S, Haase A (2003). High-resolution MRI with cardiac and respiratory gating allows for accurate in vivo atherosclerotic plaque visualization in the murine aortic arch. *Magn Reson Med*. **50**:69–74.
- Nahrendorf M, Hiller KH, Hu K, Ertl G, Haase A, Bauer WR (2003). Cardiac magnetic resonance imaging in small animal models of human heart failure. *Med Image Anal*. **7**:369–375.
- Brau ACS, Wheeler CT, Hedlund LW, Johnson GA (2002). The fiber optic stethoscope: A cardiac monitoring and gating system for magnetic resonance microscopy. *Magn Reson Med*. **47**:314–321.
- Lecomte R, Croteau E, Gauthier M-E, Archambault M, Aliaga A, Rousseau J, Cadorette J, Leroux J-D, Lepage MD, Benard F, Bentourkia M (2004). Cardiac PET imaging of blood flow, metabolism, and function in normal and infarcted rats. *IEEE Trans Nucl Sci*. **51**:696–704.
- Vanhove C, Lahoutte T, Defrise M, Bossuyt A, Franken PR (2004). Reproducibility of left ventricular volume and ejection fraction measurements in rat using pinhole gated SPECT. *Eur J Nucl Med Mol Imaging [Internet]*.
- Yang XP, Liu YH, Rhaleb NE, Kurihara N, Kim HE, Carretero OA (1999). Echocardiographic assessment of cardiac function in conscious and anesthetized mice. *Am J Physiol*. **277**:H1967–H1974.
- Camici PG (2003). Gated pet and ventricular volume. *J Nucl Med*. **44**:1662.
- Yea Y, Zhu J, Wang G (2004). Geometric studies on variable radius spiral cone-beam scanning. *Med Phys*. **31**:1473–1480.
- Badea CT, Hedlund LW, Johnson GA (2004). Micro-CT with respiratory and cardiac gating. *Med Phys*. **31**:3324–3329.
- Badea CT, Hedlund LW, Wheeler CT, Mai W, Johnson GA (2004). Volumetric micro-CT system for in vivo microscopy. *Proc IEEE Int Symp Biomed Imaging*. 1377–1381.
- Paulus MJ, Gleason SS, Easterly ME, Foltz CJ (2001). A review of

- high-resolution X-ray computed tomography and other imaging modalities for small animal research. *Lab Anim [NY]*. **30**:36–45.
- [16] Wang G, Vannier M (2001). Micro-CT scanners for biomedical applications: An overview. *Adv Imaging*. **16**:18–27.
- [17] Holdsworth DW, Thornton M (2002). Micro-CT in small animal and specimen imaging. *Trends Biotechnol*. **20**:S34–S39.
- [18] Gewalt SL, Glover GH, Hedlund LW, Cofer GP, MacFall JR, Johnson GA (1993). MR microscopy of the rat lung using projection reconstruction. *Magn Reson Med*. **29**:99–106.
- [19] Mai W, Badea CT, Wheeler CT, Hedlund LW, Johnson GA (in press). Effects of breathing and cardiac motion on the spatial resolution in microscopic imaging of rodents. *Magn Reson Med*.
- [20] Feldkamp IA, Davis LC, Kress JW (1984). Practical cone-beam algorithm. *J Opt Soc Am A*, 612–619.
- [21] Hedlund LW, Johnson GA (2002). Mechanical ventilation for imaging the small animal lung. *ILAR J*. **43**:159–174.
- [22] Hedlund LW, Cofer GP, Owen SJ, Allan Johnson G (2000). MR-compatible ventilator for small animals: Computer-controlled ventilation for proton and noble gas imaging. *Magn Reson Imaging*. **18**:753–759.
- [23] Weichert JP, Lee FT Jr, Longino MA, Chosey SG, Counsell RE (1998). Lipid-based blood pool CT imaging of the liver. *Acad Radiol*. **5**:S16–S19.
- [24] Weichert JP, Bjorling DE, Moser AR, Durkee BY, Longino MA, Lee FT Jr. (2003). Virtual microCT angiography with bp20 in live mice. Contrast Media Research '03. San Diego, CA.
- [25] Rose A (1948). The sensitivity performance of the human eye on an absolute scale. *J Opt Soc Am*. **38**:196–208.
- [26] Lipton MJ, Higgins CB, Boyd DP (1985). Computed tomography of the heart: Evaluation of anatomy and function. *J Am Coll Cardiol*. **5**:55S–69S.
- [27] Vera DR, Mattrey RF (2002). A molecular CT blood pool contrast agent. *Acad Radiol*. **9**:784–792.
- [28] Ford NL, Thornton MM, Holdsworth DW (2003). Fundamental image quality limits for microcomputed tomography in small animals. *Med Phys*. **30**:2869–2877.
- [29] Kozerke S, Tsao J (2004). Reduced data acquisition methods in cardiac imaging. *Top Magn Reson Imaging*. **15**:161–168.
- [30] Kozerke S, Tsao J, Razavi R, Boesiger P (2004). Accelerating cardiac cine 3d imaging using k-t blast. *Magn Reson Med*. **52**:19–26.
- [31] Tsao J, Boesiger P, Pruessmann KP (2003). K-t blast and k-t sense: Dynamic MRI with high frame rate exploiting spatiotemporal correlations. *Magn Reson Med*. **50**:1031–1042.
- [32] Cody DD, Cavanaugh D, Price RE, Rivera B, Gladish G, Travis E (2004). Lung imaging of laboratory rodents in vivo. **5535**:43–52.